Polish J. Chem., **76**, 249–262 (2002)

Photoconduction in the Metal Chelate Tris-(8-hydroxyquinolinato) Aluminum (Alq_3)*

by J. Kalinowski, W. Stampor and J. Szmytkowski

Department of Molecular Physics, Technical University of Gdańsk, ul. G. Narutowicza 11/12, 80-952 Gdańsk, Poland

(Received May 28th, 2001; revised manuscript August 6th, 2001)

Electric field, light wavelength and excitation intensity characteristics of photoconduction have been measured in an aluminum (Al)/tris-(8-hydroxyquinolinato) aluminum(III) (Alq_3)/Al sandwich system. The results show the photocurrent to be underlain by intrinsic dissociation of singlet excited states (Alq_3^*) into a pair of free electrons and holes. However, conventional theories, such as Onsager or Poole-Frenkel models for charge photogeneration cannot account for the experimentally observed characteristics. Excellent agreement with experiment is provided by the 3D-Onsager theory of geminate recombination combined with volume (bimolecular) recombination of the photogenerated space charge. This model predictions are also consistent with independent electric field-induced fluorescence quenching experiments and are able to account for the decrease in the electroluminescence quantum efficiency of Alq_3-based organic light-emitting diodes at high electric fields.

Key words: photoconduction in organics, electromodulation spectroscopy, dissociation of excitons, charge carrier recombination, organic light emitting diodes

The metal chelate tris-(8-hydroxyquinolinato) aluminum(III) (Alq_3) has become one of the most studied organic material since its first use as an emitter (EM) and electron transporter (ET) in organic light-emitting diodes (LEDs) [1,2]. The fact that it is still the most widely used as EM and ET layers in organic LEDs [3,4] proves the great technological importance of this compound. In typical Alq_3 emitter-based LEDs, light occurs as a result of the radiative relaxation of molecular excitons (Alq_3^*) produced *via* the bimolecular recombination of electrons (e) and holes (h) injected from electrodes [4]. The quantum electroluminescence (EL) efficiency (φ_{EL}) of such LEDs appears to be a function of their operational parameters including applied electric field (F). $\varphi_{EL}(F)$, initially increases at low fields (LF), reaches a maximum value then decreases at high fields (HF) [5]. The field-assisted exciton dissociation has been invoked to explain the drop of $\varphi_{EL}(F)$ at high electric fields [5,6]. The existence of such a process should be directly observed as photoconduction (PC) excited by light within the first absorption band.

---

*Dedicated to the memory of Professor Krzysztof Pigoń.

In this paper we report results from steady-state photoconduction that show field, light intensity and spectral characteristics indicative of the intrinsic photogeneration of charge from the first optically-excited singlet state in solid films of Alq_3. These results are consistent with the data for the field-induced quenching of fluorescence, and are able to account for the decrease in the EL quantum efficiency of Alq_3-based LEDs at high electric fields.

EXPERIMENTAL

Films of Alq_3, about 0.5–2 μm thick, measured by profilometry, were prepared by thermal vacuum ($\cong 10^{-4}$ Pa) evaporation at a rate 0.3–0.4 nm s^{-1} onto quartz or glass slides covered by a semitransparent thin layers of Al. A sandwich structure was formed by vacuum deposition of a semitransparent Al top electrode without breaking vacuum in order to inhibit atmospheric oxidation of the electrode. Deposition was carried out by thermal evaporation from a Ta boat at a nominal deposition rate of 2–4 nm/s. The thickness of the metal coatings was determined by measurements of the optical transmittance, in the range 20%–50%; an additional substrate was placed in the evaporation setup and the optical transmission control unit used during the formation of the films. The electrical contacts between metal films and the external electrical leads were made by small drops of silver epoxy (Fig. 1a). Alq_3 (Fig.1b) was purchased from

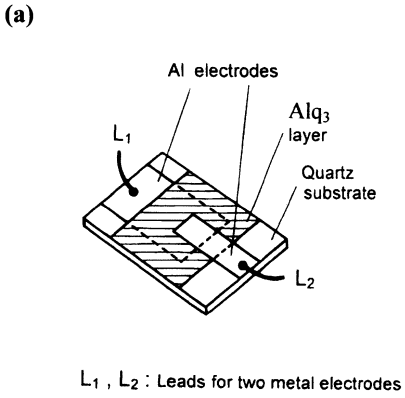

Figure 1. Sandwich configuration of the samples (a) and molecular structure of Alq_3 (b).

Aldrich and was used as is or purified by sublimation. No systematic difference was observed in the experimental data obtained with such purified material and that used without further purification. The electric field modulated fluorescence was studied using a sinusoidal field with the frequency $\omega/2\pi = 175$ Hz applied to the sample as described in [7]. The field amplitude ranged between 10^5 and 2×10^6 V cm^{-1}. The steady-state PC measurements were conducted by irradiation either side of the Alq_3 films sandwiched between two semitransparent Al layers, which could be either positively or negatively biased electric contact. A Narva 200 W Mercury lamp and an Osram 150 W Xenon lamp were used as light sources. The active electrode area of the film was typically 0.1 cm^2. The photocurrent was measured within the quantal intensity range $10^{11} < I_o < 10^{15}$ quanta/cm^2 s and a d.c. field range between 10^3 and 1.5×10^5 V cm^{-1}. The action spectra of the photocurrent were measured between 300 and 500 nm, comprising the penetration depth between 197 nm ($\lambda = 390$ nm) and 21 μm ($\lambda = 500$ nm). All measurements were carried out in ambient atmosphere conditions.

RESULTS AND DISCUSSION

Dark conductivity: Current-field responses of the cells in the dark showed the symmetry as far as the bias of the non-substrate or substrate electrode is concerned. The results for j_{dark} plotted as log j_{dark} against log F and in the log $j_{dark} - F^{1/2}$ scale show the current to obey the Schottky-type relationship, $j_{dark} = j_0 \exp(aF^{1/2})$, with $a_{exp} = 0.77\times10^{-2}$ (cm/V)$^{1/2}$ (Fig. 2). This value of a_{exp} is in excellent agreement with the $a_{theor} = (e/kT)(e/4\pi\varepsilon_o\varepsilon)^{1/2} = 0.78\times10^{-2}$ (cm/V)$^{1/2}$ [3,4] as calculated for ($T \cong 300$ K), and with $\varepsilon = 3.8$ [8]. Deviations from the power law, $j_{dark} \sim F^n$ with $n \geq 2$, seems to rule out the space-charge-limited current (SCLC), thus, the $j_{dark}(F)$ characteristics reflects the field dependence of the majority carrier Schottky-type injection rather than of trans-

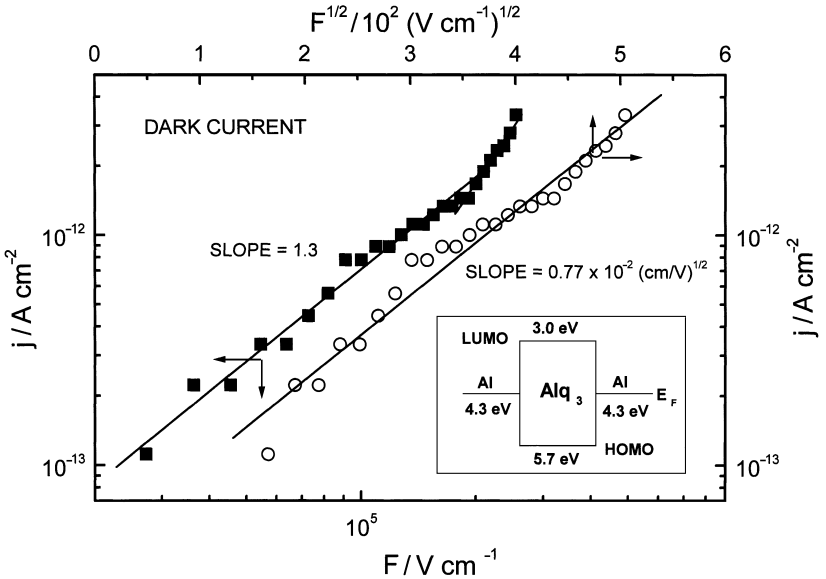

Figure 2. Field dependence of the dark current for the Al^+/Alq_3(1.1 μm)/Al^-/glass sample in two representations: log j *versus* log F (squares), and log j *versus* $F^{1/2}$ (circles). The full straight lines, with indicated slopes, are power ($j_{dark} \sim F^n$), and Schottky-type [$j_{dark} \sim \exp(aF^{1/2})$] approximations, respectively. Energy level relationships at the interface of Al electrode and Alq_3 interface are given in the inset.

port [3,4]. This conclusion is strongly supported by the low current. For example, $j = 10^{-12}$ A/cm^2 leads to the carrier concentrations on the order of $n = j/e\mu F \cong 10^8$ cm^{-3} with the mobility ascribed to the faster carriers (electrons), $\mu = \mu_e = 5\times10^{-7}$ cm^2/Vs (see below the following discussion on the role of positive and negative charge carriers), at $F = 10^5$ V/cm. The SCLC limit for the carrier concentration would give $n \cong \varepsilon_o\varepsilon F/ed \cong 10^{15}$ cm^{-3}, that is a value seven orders of magnitude larger. Since the high injection barriers for holes ($\Delta E_h \cong 1.4$ eV), and for electrons ($\Delta E \cong 1.3$ eV) at the Al/Alq_3 interface are equal within the accuracy of the energy level positions (see the inset in Fig. 2), one would expect a balanced, yet very inefficient, injection of both holes and electrons.

Photoconduction and electromodulation optical measurements: In Fig. 3 a comparison is given between photocurrents (j) measured on samples with positive and negative bias of the non-substrate illuminated electrode. The positive (j_+) and

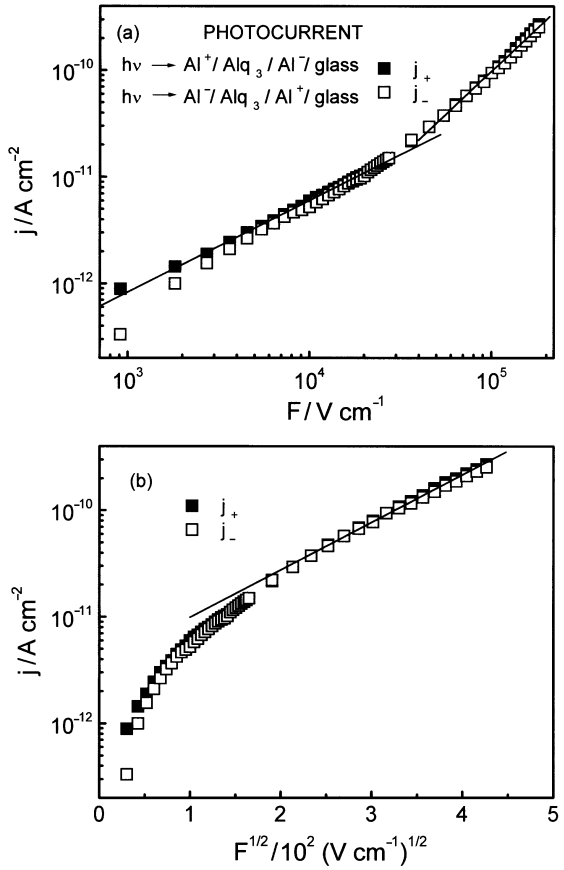

Figure 3. Steady-state photocurrent as a function of applied field for the sample from Fig. 2, illuminated through the positively (j_+; full squares) and negatively (j_-; open squares) biased non-substrate electrode. The results are plotted in two different representations: (a) log j *versus* log F, and (b) log j *versus* $F^{1/2}$. The photocurrents obtained with a photon flux per unit area $I = 10^{13}$ quanta/cm^2 s at excitation wavelength 430 nm.

negative (j_-) photocurrents are practically identical and exceed the dark current by about two orders of magnitude (*cf.* Fig. 2). Deviations from the power function ($j \sim F^n$, $n \geq 2$) and Schottky-like behavior [$j \sim \exp(aF^{1/2})$ approximating the high field segment with $a_{exp} \cong 10^{-2}$ $(cm/V)^{1/2}$] indicate that either SCLC and 1D version of the Onsager theory of excitonic injection mechanisms [9] can be disregarded, and suggesting the photocurrent to be controlled by an intrinsic photogeneration process. A possible mechanism for the photogeneration of carriers in solid Alq_3 is that the excited singlet states (Alq_3^*) may dissociate into separated electrons and holes, in addition to the radiative relaxation producing fluorescence, $h\nu_{fl}$. This is shown in some detail in Fig. 4. The initial separation step involves a charge-transfer state (CT) formed with a field independent probability, η_o, and a field-depending CT dissociation process (Ω) into separated charge carriers (e + h). Thus, the photocurrent can be expressed as

$$j = e\eta I \tag{1}$$

where η is the overall probability for excited states to dissociate into separated charge carriers, and I the quantal exciting light intensity (photons/cm^2 s). At low fields, the experimental photogeneration efficiency (j_{exp}/eI) is very low, extrapolated to F = 0 gives $\eta(0) < 10^{-6}$ (Fig. 5).The field-dependent photogeneration efficiency is compared with theoretical predictions neglecting the back volume recombination (η_{VR}), $\eta(F) = \eta_o\Omega(F)$, as often met [10–14]. It turns out that the majority of the experimental data are between the predictions of the conventional Onsager 38 model [15] and the earlier Onsager model [16] as modified by Braun (Braun 84 [17]), apparently, the Poole-Frenkel (PF) formalism [18] giving the best fit within the 10^3–10^5 V cm^{-1} field range. The fitting curve has been calculated by the PF expression for the quantum photogeneration yield [19],

$$\eta_{PF} = \eta_o \frac{\exp(\beta_{PF} F^{1/2})}{A_{PF} + \exp(\beta_{PF} F^{1/2})} \tag{2}$$

with $\eta_o = 1.0$, $\beta_{PF} = (e^3/\pi\varepsilon_o\varepsilon k^2T^2)^{1/2} = 1.6\times10^{-2}$ $(cm/V)^{1/2}$ ($\varepsilon = 3.8$ [8]) and $A_{PF} = 5\times10^5$, the latter expressing the recombination-to-generation rate constants ratio at F = 0.

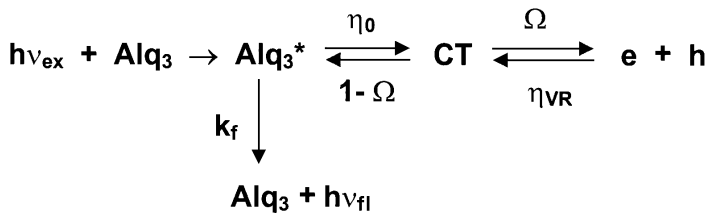

Figure 4. Photo-excitation and dissociation of Alq_3^* leading to the charge transfer state (CT) and electron-hole pairs, the latter giving rise to photocurrent flowing in solid Alq_3.

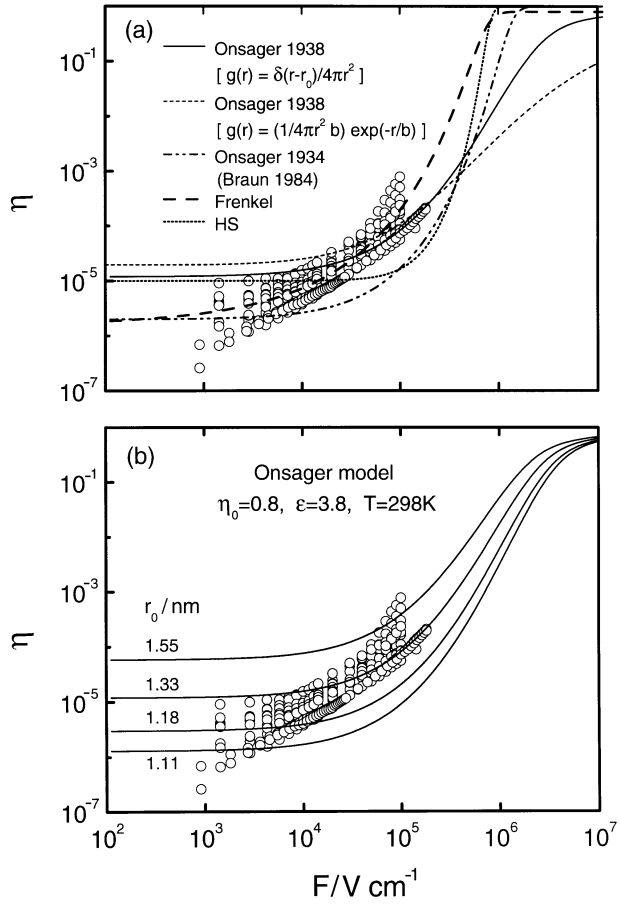

Figure 5. Field-dependent quantum efficiencies for five different samples, taken at three excitation wavelengths, 313 nm, 366 nm and 430 nm. Their values were obtained from experimental values of j_+ and j_-. The quantal excitation intensity was $I = 10^{13}$ ph/cm^2 s, and the sample thicknesses ranged between 0.7 and 1.1 μm. The lines represent theoretical predictions of $\eta(F)$ for different models (a), and the conventional 1938 Onsager model with different values of the initial charge carrier separation, r_o, (b). The Onsager curves in part (a) were calculated with r_o = 1.6 nm and $\eta_o = 0.8$ (solid line), and b = 0.4 nm, $\eta_o = 0.8$ (dash-dotted line; Braun 1984). The HS curve follows the function $\eta(F) = \sinh(\beta F)[A_M + \sinh(\beta F)]^{-1}$ [19] with $\beta = 0.18$ μm V^{-1} and $A_M = 10^5$. All the models ignore the back volume recombination η_{VR} (*cf.* Fig. 4).

However, the PF approach predicts the saturation value of η ($\eta = 1$) for electric fields below 10^6 V cm^{-1} at variance with the experimental data resulting from electrical measurements for other compounds [12,14] and electromodulated fluorescence (EMF) measurements for Alq_3 [7] (see also Fig. 8). Furthermore, like other models of strictly photogeneration controlled currents, the PF approach fails to explain the light intensity and excitation spectrum of the photocurrent as presented and discussed later in this section. Figure 5 shows the hopping separation (HS) model [7,19] of photodissociation efficiency to be inadequate to justify the experimental results as well.

Also, modifying the Onsager 38 model by introduction of an exponential distribution function for the initial electron-hole separation (r), $g(r) = (4\pi r^2 b)^{-1}\exp(-r/b)$ [20] does not allow to predict correctly the experimental data for $\eta(F)$ (Fig. 5a).

The major problem with application of the conventional 1938 Onsager theory is the weak initial field dependence of $\eta(F)$. It cannot be resolved by variation of neither r_o nor b. A set of theoretical curves computed according to the conventional Onsager 38 model is shown in Fig. 5b. The computation has been performed using the integral of the Onsager function $f(r,\theta)$ over space [21],

$$\eta(F) = \eta_o \Omega(F) = \eta_o \int g(r,\theta) f(r,\theta) d\tau \tag{3}$$

where $g(r,\theta)$ is the probability per unit volume of finding the ejected electron in a volume element $d\tau$ at θ,r for the specific ionization process, and,

$$f(r,\theta) = \exp[-(A+B)] \sum_{m}^{\infty} \sum_{n=0}^{\infty} \frac{A^m}{m!} \frac{B^{m+n}}{(m+n)!} \tag{4}$$

with $A = 2q/r$, $B = \beta r(1 + \cos\theta)$, $q = e^2/8\pi\varepsilon_o\varepsilon kT$, $\beta = eF/2kT$. $g(r,\theta)drd\theta \cong 4\pi r^2 g(r)dr$ with $g(r) = \delta(r - r_o)/4\pi r_o^2$ has been assumed, and $\varepsilon = 3.8$ and $kT = 0.025$ eV used in the calculation [19]. As may be seen, variation of r_o between 1.11 nm and 1.55 nm practically does not change the flat shape of the low-field part of the $\eta(F)$ function.

All theoretical curves presented in Fig. 5 have been computed under the tacit assumption that there exists a homogeneous electric field distribution inside the layers, despite the space charge expected to be of particular significance at low fields. A direct proof for the existence of internal fields comes from the non-zero first harmonic signal in electroabsorption (EA) spectra [22]. The results of our EA studies performed on Alq_3 films show a linear field increase of the EA signal, $(\Delta I/I)_{1\omega}$, at the first harmonic (1ω) (Fig. 6a) and a quadratic field increase of the EA signal, $(\Delta I/I)_{2\omega}$, at the second harmonic (2ω) (Fig. 6b). Their ratio [23]

$$\left|(\Delta I/I)_{1\omega}\right| / \left|(\Delta I/I)_{2\omega}\right| = \left|-4F_i/F_o\right| \tag{5}$$

allows to determine the internal electric field, F_i, at a given a.c. applied electric field expressed by its amplitude F_o. From the data of Fig. 6, $F_i = 0.5\times10^5$ V cm^{-1} follows for $U_{rms} = 80$V ($F_o = 2.06\times10^6$ V cm^{-1}). It varies with wavelengths but its order of magnitude falls always in the low field region of the experimental η-F plots. Thus, it is obvious that the exciton dissociation process proceeds under an effective field being a sum of the internal and external field applied to the sample. Figure 7 presents the application of the 1938 Onsager theory to the experimental results for different internal fields. Again, the results are substantially different from the theoretical predictions. The photogeneration efficiencies predicted from the theory do not recover their experimental values in the low field region, and approach unity at very high fields ($\cong 10^7$

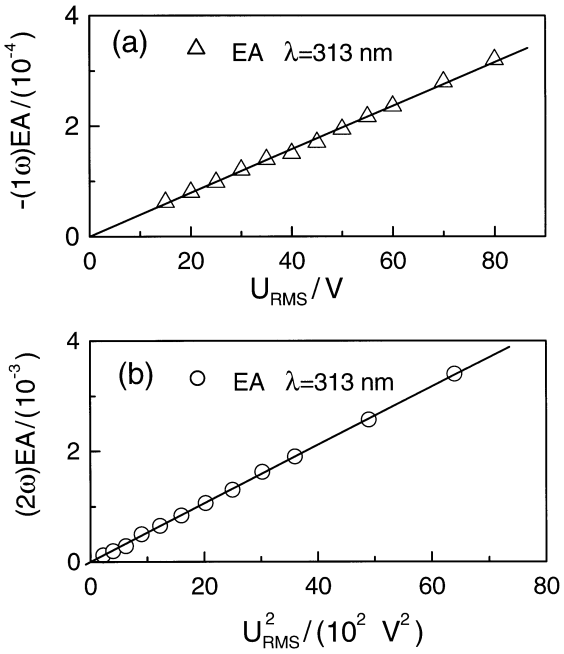

Figure 6. EA signal detected at the first (1ω) and second (2ω) harmonics as a function of the rms voltage applied to the Alq_3 sample of thickness d = 0.55 μm. The data obtained at 313 nm.

V cm^{-1}). From the above discussion it can be concluded that none of the existing photogeneration models, including their versions with a space-charge modified local fields, are able to recover the experimental photogeneration results for solid Alq_3 films at fields below 10^5 V cm^{-1}. In order to determine the photocurrent we invoke the volume recombination (VR) to reduce the effective (overall) photogeneration efficiency, and to provide a means to derive its electric field dependence,

$$\eta = \eta_o \Omega(F)[1 - \eta_{VR}(F)] \tag{6}$$

The bimolecular recombination efficiency (η_{VR}) is determined by the recombination time, τ_{rec}, and transit time, τ_t, of the carriers to the electrodes,

$$\eta_{VR} = (1 + \tau_{rec}/\tau_t)^{-1} \tag{7}$$

with $\tau_{rec} = (\gamma n_h)^{-1} \cong \varepsilon_o \varepsilon / e\mu_e n_h$, and $\tau_t \cong (d/2)/\mu_e F$, where n_h is the concentration of holes, and d is the sample thickness. The final form of τ_{rec} has been obtained assuming Langevin mechanism of the recombination of more mobile (μ_e) electrons [24] and less mobile (μ_h) holes [25], $\gamma \cong e\mu_e/\varepsilon_o\varepsilon$. This renders the space charge to be dominated by holes ($n_{tot} \cong n_h$). Consequently,

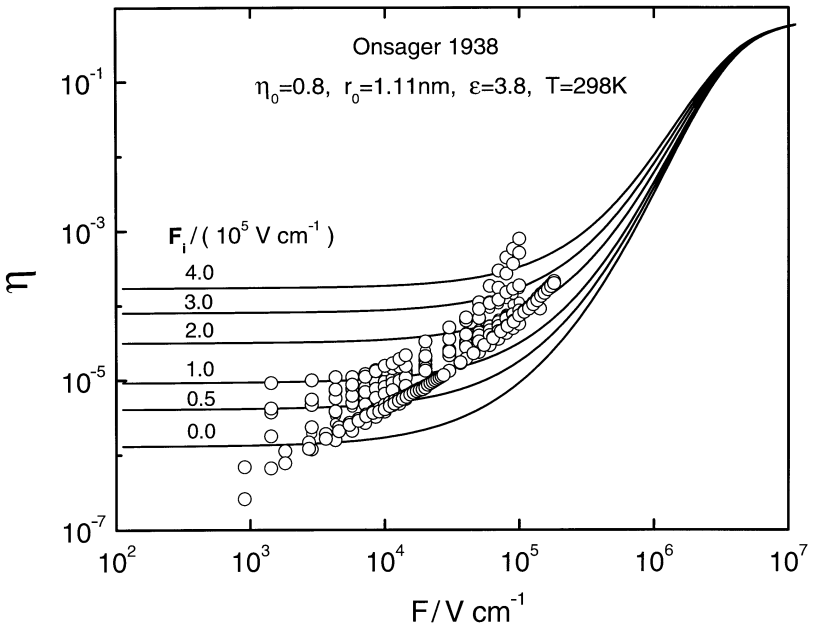

Figure 7. Field dependence of the photogeneration efficiency (figures) as compared with the 1938 Onsager theory curves parametric in the internal field, F_i.

$$\eta_{VR} = (1 + 2\varepsilon_o\varepsilon F/en_h d)^{-1} \tag{8}$$

and

$$\eta = \eta_o\Omega\,(F)(1 + edn_h/2\varepsilon_o\varepsilon F)^{-1} \tag{9}$$

Figure 8 shows experimental field-dependent quantum photogeneration efficiencies determined from photocurrent data for five different samples, and from EMF measurements for two different samples. The best curve fit according to (9), assuming $\eta_o\Omega(F)$ to follow the conventional 1938 Onsager theory, is represented by the solid line. The theoretical curve fits the data well at all applied fields if the space charge (n_{tot}) and η_{VR} decrease with applied field as shown in the inset of Fig. 8. For $n_h \leq 10^{15}$ cm^{-3}, the second term in the denominator of (9) is much smaller than unity and $\eta \cong \eta_o\Omega(F)$. The physical meaning of this result is that in the low-field region the discharge of the carriers at their exit contacts is not efficient enough to suppress volume recombination (the recombination-to-transit time ratio is less than or comparable with unity). At higher fields the space charge is reduced due to the more efficient hole discharge at the cathode, caused by increasing carrier mobilities [24,25] and the applied field itself. As a result, the concentration of charge becomes predominantly controlled by the charge separation efficiency in accord with the Onsager 38 formalism as shown in Fig. 8 by the dashed line.

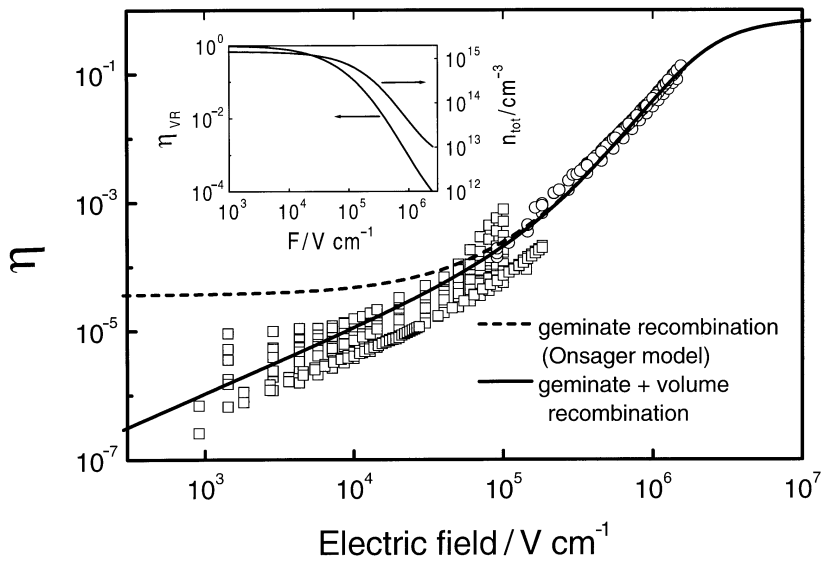

Figure 8. Electric field dependence of carrier generation efficiency for eight different samples of Alq_3. Squares represent steady-state photoconduction measurements for five samples, and circles represent fluorescence quenching measurements for three samples. The dashed line was calculated using the conventional 1938 Onsager theory with $g(r) = \delta(r - r_o)/4\pi r^2$, assuming $r_o = 1.5$ nm and $\eta_o = 0.8$. The solid line is the prediction using the scheme in Fig. 4, plotted according to Eq. (9). The field evolution of the bimolecular recombination efficiency (η_{VR}) and the total concentration of holes (n_h) used in the fitting procedure are given in the inset.

It is worthy to note that the electron concentration related to the concentration of holes, $n_e/n_h \cong 10^{-3}$ ($n_e \cong j_{ph}/e\mu_e F \cong 10^{11}$ cm^{-3} at F = 10^5 V cm^{-1}, using $\mu_e \cong 5\times10^{-7}$ cm^2/Vs [24]) is about one order of magnitude lower than the ratio $\mu_h/\mu_e \cong 10^{-2}$ resulting from the independent time-of-flight (TOF) mobility data for electrons [24] and holes [25] in Alq_3. This indicates hole traps to be distributed in energy with the distribution tail extended towards deep trapping levels. The time, spent by a hole in such traps, exceeds its transit time, thus, it cannot be detected in the TOF type mobility measurements. Assuming for the thermal release time, $\tau_{rel} = \nu^{-1}\exp(\Delta E/kT)$, of the carrier, the transit time as an upper limit, $\tau_t \cong (d/2)/\mu_h F \cong 0.3$ s ($\mu_h \cong 2\times10^{-9}$ cm^2/Vs at F = 10^5 V cm^{-1} [25]), the lower limit of the deep trap depth can be evaluated assuming a suitable value for the attempt-to-escape frequency factor ν. With, typically, $\nu = 10^{12}$ s^{-1}, $\Delta E \geq 0.66$ eV which would agree with $\Delta E \cong 0.8$ eV revealed from thermally stimulated current (TSC) studies [26]. A low value of $\nu \cong 10^5$ s^{-1} would be required to get the $\Delta E \cong 0.25$ eV limit as found from the thermally stimulated luminescence spectrum of 100 nm thick Alq_3 films [27].

Apart from demonstrating the general mutual consistency of the VR-modified photogeneration efficiency (9) and experimental results, the latter show a relatively large scatter in the photocurrent data for different samples, varying excitation wavelength and intensities (Fig. 8). The essential model parameter at low fields is the con-

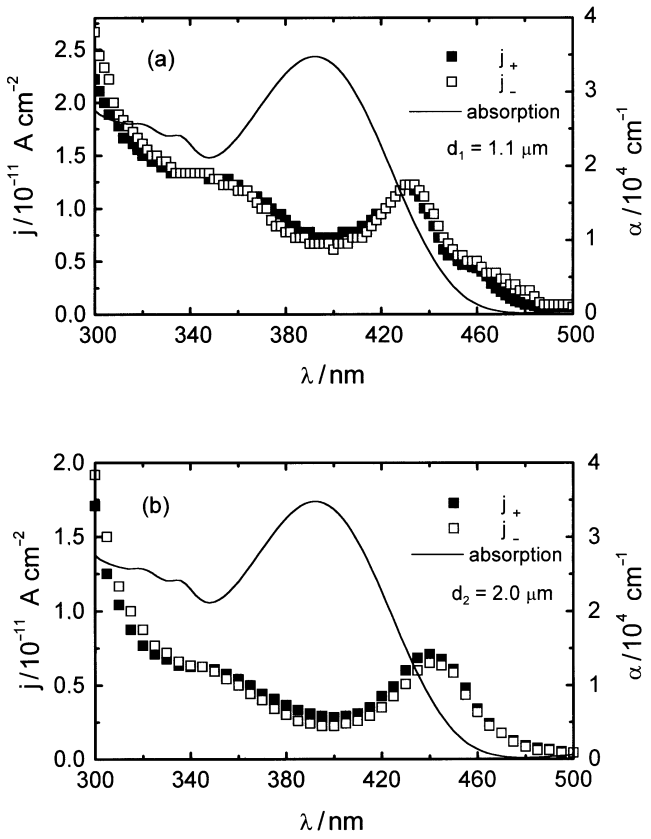

Figure 9. Photocurrent (j_+ and j_-) action spectra for two different thickness Alq_3 films. All photocurrent spectra correspond to room temperature for different set of electrical and optical parameters. (a) $F = 10^5$ V cm^{-1}, $I = 2\times10^{12}$ ph/cm^2 s; (b) $F = 10^4$ V cm^{-1}, $I = 1.3\times10^{13}$ ph/cm^2 s.

centration of space charge that causes variation of $\eta(F)$ due to the term $edn_h/2\varepsilon_o\varepsilon F$ in (9). It is for this reason that the photocurrent behaves slightly antibatically with absorption (Fig. 9) and is sublinear with light intensity (Fig. 10). An additional reason for this scatter is space-charge imposed modification of local electric fields, where the major part of dissociation events occur. Given the observed sublinear increase of photocurrent with increasing light intensity, the light intensity dependence of the space charge $n_h(I)$ can be extracted from (1) substituting η with (9),

$$j = e\eta_o\Omega(F)I(1 + edn_h/2\varepsilon_o\varepsilon F)^{-1} \tag{10}$$

An example presented in the inset of Fig. 10 shows the space charge to follow approximately a sublinear dependence $n_{tot}(I) \sim I^m$ with $m \cong 0.2$. This curve, within the experimentally attainable range of I, merges with the function

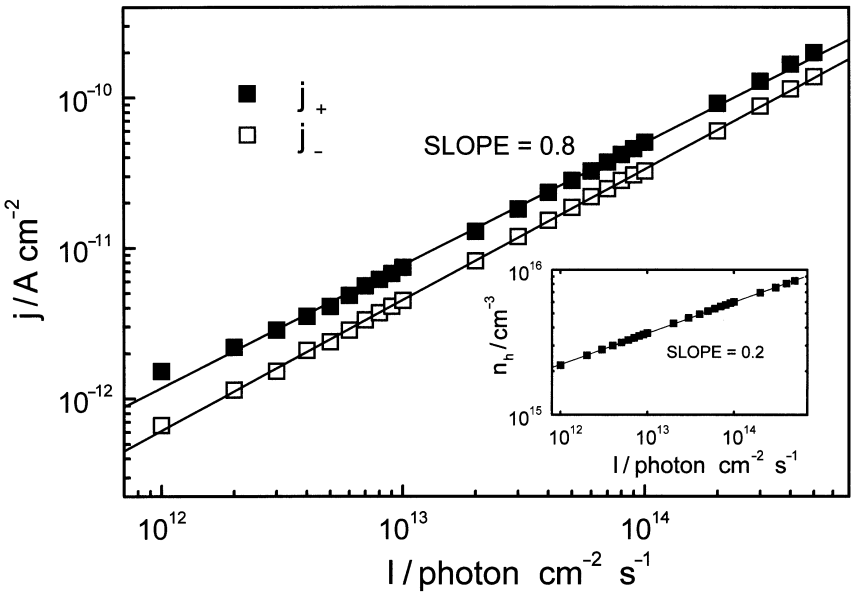

Figure 10. Light intensity dependence of the "positive" (j_+) and "negative" (j_-) photocurrents at excitation wavelength 313 nm, and $F = 10^4$ V cm^{-1} for a 1.3 μm thick Alq_3 film. Inset: Light intensity evolution of the space charge underlying the light intensity dependence of the photocurrent according to Eq. (10). The lines are guides to the eye and are meant to indicate a log-log straight-line approximations of the $j \sim I^n$ with $n \cong 0.8$, and $n_h \sim I^m$ with $m \cong 0.2$.

$$n_h = [(ed/2\varepsilon_o\varepsilon F) + (2\mu_h F/\alpha Id)]^{-1} \quad (11)$$

resulting from the kinetics of electrons and holes of which holes decay in both VR and electrode discharge processes, whereas the electron decay is dominated by the electrode discharge due to their much larger mobility. In (11) μ_h is the hole mobility and α denotes the absorption coefficient of the exciting light.

The action photocurrent spectra are difficult to interpret quantitatively. The main feature between 430 and 440 nm can be assigned to the penetration depth of the exciting light $l_a \cong 1$ μm, at which the number of absorbed photons becomes a decreasing function of wavelength, due to the light transmission through the sample. Its position is expected then to shift towards the long-wavelength tail of the absorption spectrum as thickness of the sample increases. In fact, this can be seen for the different sample thickness action spectra displayed in Figs. 9a and 9b. A slightly antibatic behavior of the photocurrent within the main absorption band peaking at ≅ 392 nm comes from the penetration depth dependence of the spatial distribution of the space charge. The shallower penetration of the exciting light is, the higher concentration of the space charge is, leading to lower values of the photocurrent. A generally symbatic photocurrent response to the absorption spectrum in the short-wavelength range might be associated with the photon energy dependence of the photocurrent rather than with the penetration depth evolution of the space charge. Examples presented in Fig. 9

have been selected in a way to show also a difference in the photocurrent values imposed additionally by excitation intensity and the field applied to the sample. It can be as high as a factor of 1.5 at ≅ 400 nm and approaching zero at ≅ 300 nm. In other samples, photocurrents (not shown in Fig. 9) can exceed these values by about an order of magnitude, reflecting the large scatter of the results for η(F) displayed in Fig. 8.

Application to the EL efficiency: The field-assisted dissociation of singlet excitons reduces the emission efficiency by a factor $(1 - \eta)$. Hence, the probability that an excited state, Alq_3^*, relaxes radiatively is $P_{fl} = [k_f/(k_f + k_n)](1 - \eta)$, k_n being the rate constant for non-radiative decay pathways other than exciton dissociation. Using the experimental value of the absolute PL efficiency $\varphi_{PL} = k_f/(k_f + k_n) = 25\%$ [5], $P_{fl} = 0.23$ is obtained with $\eta = 0.07$ at a field ≅ 10^6 V cm^{-1} (see Fig. 8). This would lead to about 10% drop of φ_{EL} in a neat Alq_3 emitter-based LED. The φ_{EL} decrease in such a LED, defined as $[\varphi_{EL}^{(max)} - \varphi_{EL}(F)]/\varphi_{EL}^{(max)}$ has been found to be on the order of ≅ 20% at F about 10^6 V cm^{-1} [5], which agrees roughly with the above prediction.

Concluding remarks: The electric field-, light intensity- and wavelength-dependent photoconduction of solid Alq_3 sandwiched between two semitransparent Al electrodes has been shown to be underlain by an intrinsic photogeneration mechanism. The results have been analyzed by a kinetic model for electric field-assisted dissociation of singlet excited states, Alq_3^*, into free charge carriers, based on Onsager's 1938 theory combined with the volume (bimolecular) recombination of the separated charges. The best fit of the theoretical model to experiment is obtained if one assumes an electric field decreasing, and light intensity increasing concentration of the space charge. For the system studied, a Coulombic interaction for the electron-hole pair shows the most probable charge-transfer radius of 1.5 nm, the quantum yield of charge transfer states $\eta_o = 0.8$, and $\eta(F = 0) = 4\times10^{-5}$. The space charge reducing η by the back volume recombination is found to be of the order 10^{15} cm^{-3}. The role of the volume recombination becomes negligible at high fields (> 10^5 V cm^{-1}), where the field dependence of the photogeneration efficiency, extracted from both electrical and EMF experiments follows well 3D-Onsager's 1938 theory, solely. Finally, the field dependent fluorescence quenching allows one to evaluate the high-field decrease in the EL quantum efficiency of the Alq_3 emitter-based LEDs as due to Alq_3^* dissociation into free carriers.

Acknowledgment

This work has been performed under partial support of the Department of the US Navy, Office of Naval Research (ONR).

REFERENCES

1. Tang C.W. and VanSlyke S.A., *Appl. Phys. Lett*., **51**, 913 (1987).
2. Tang C.W., VanSlyke S.A. and Chen C.H., *J. Appl. Phys*., **65**, 3610 (1989).
3. *Organic Electroluminescent Materials and Devices*, Eds. Miyata S. and Nalwa H.S., Gordon & Breach, Amsterdam 1997.
4. Kalinowski J., *J. Phys. D: Appl. Phys*., **32**, R179 (1999).

5. Kalinowski J., Picciolo L.C., Murata H. and Kafafi Z.H., *J. Appl. Phys*., **89**, 1866 (2001).
6. Kalinowski J., Cocchi M., Fattori V., Di Marco P. and Giro G., *Jpn. J. Appl. Phys*., **40**, L282 (2001).
7. Stampor W., Kalinowski J., Di Marco P. and Fattori V., *Appl. Phys. Lett*., **70**, 1935 (1997).
8. Kalinowski J., Camaioni N., Di Marco P., Fattori V. and Martelli A., *Appl. Phys. Lett*., **72**, 513 (1998).
9. Godlewski J. and Kalinowski J., *Jpn. J. Appl. Phys*., **28**, 24 (1989).
10. Chance R.R. and Braun C.L., *J. Chem. Phys*., **59**, 2269 (1973).
11. Braun C.L. and Chance R.R., in *Energy and Charge Transfer in Organic Semiconductors*, Eds. Masuda K. and Silver M., Plenum Press, NY 1974.
12. Borsenberger P.M. and Ateya A.I., *J. Appl. Phys*., **49**, 4035 (1978).
13. Borsenberger P.M., Contois L.E. and Hoesterey D.C., *J. Chem. Phys*., **68**, 637 (1978).
14. Cimrová V. and Nešpůrek S., *Chem. Phys*., **184**, 283 (1994).
15. Onsager L., *Phys. Rev.*, **54**, 554 (1938).
16. Onsager L., *J. Chem. Phys*., **2**, 599 (1934).
17. Braun C.L., *J. Chem. Phys*., **80**, 4157 (1984).
18. Frenkel J., *Phys. Rev.*, **54**, 647 (1938).
19. Kalinowski J., Stampor W. and Di Marco P., *J. Chem. Phys*., **96**, 4136 (1992).
20. Borsenberger P.M. and Ateya A.I., *J. Appl. Phys*., **50**, 909 (1979).
21. Pope M. and Swenberg C.E., *Electronic Processes in Organic Crystals*, Clarendon Press, Oxford 1982, p. 484.
22. Stampor W., Kalinowski J. and Di Marco P., *Chem. Phys*., **134**, 385 (1989).
23. Stampor W., Kalinowski J. and Di Marco P., *Mol. Cryst. Liq. Cryst*., **228**, 233 (1993).
24. Barth S., Müller P., Riel H., Seidler P.F., Riess W., Vestweber H. and Bässler H., *J. Appl. Phys*., **89**, 3711 (2001).
25. Naka S., Okada H., Onnagawa H., Kido J. and Tsutsui T., *Jpn. J. Appl. Phys*., **38**, L1252 (1999).
26. Mori T., Miyake S. and Mizutani T., *Jpn. J. Appl. Phys*., **34**, 4120 (1995).
27. Forsythe E.W., Morton D.C., Tang C.W. and Gao Y., *Appl. Phys. Lett*., **73**, 1457 (1998).